Active tectonics of the onshore Hengchun Fault using UAS DTM combined with ALOS PS-InSAR time series (Southern Taiwan)

Benoit Deffontaines[1, 2], Kuo-Jen Chang[2, 3], Johann Champenois[4], Kuan-Chuan Lin[5], Chyi-Tyi Lee[2, 6], Rou-Fei Chen[2, 7], Jyr-Ching Hu[2, 5], Bénédicte Fruneau[2, 8]

[1]LAREG Unit (IGN-UDD-IPGP-UPEM), LaSTIG (IGN-UPEM), Marne-la-Vallée, 77454, France
[2]Lab. Int. Assoc. D3E N°536, CNRS-MOST France-Taiwan.
[3]Department of Civil Engineering, National Taipei University of Technology, Taipei, 10654, Taiwan
[4]Laboratoire Tectonique et Mécanique de la lithosphère, IPGP, Paris, 75005, France
[5]Department of Geosciences, National Taiwan University, Taipei, 10617, Taiwan
[6]Department of Applied Geology, Central Taiwan University, Chungli, 32001, Taiwan
[7]Departement of Geology, Chinese Culture University, Taipei, 11114, Taiwan
[8]Université Paris Est, LaSTIG, IGN, UPEM, Marne-la-Vallée, 77454, France.

Correspondence to: Kuo-Jen Chang (epidote@ntut.edu.tw)

Abstract. Characterizing active faults and quantify their activity are major concern in Taiwan, especially following the major Chichi earthquake of September 21st, 1999. Among the targets that still remain poorly known in terms of active tectonics, are the Hengchun and Kenting Faults (Southern Taiwan). From the geodynamic point of view, they affects the outcropping top of the Manila accretionary prism of the Manila subduction zone that runs from Luzon (N. Philippines) to Taiwan. In order to better settle the location and quantify the activity of the Hengchun Fault, we start from the existing geological maps, Chinese Petroleum Corporation (CPC, 1993) and Central Geological Survey (Sung, 1991) ones, which we update thanks to the use of two products derived from Unmanned Aircraft System's acquisitions : 1) the very high precision (<50 cm) and resolution (<10 cm) Digital Terrain Model (DTM), and the 2) the georeferenced aerial photograph mosaic of the studied area. Moreover, the superimposition of the resulting structural sketch map with new Persistent Scatterers (PS) - InSAR results obtained from PALSAR ALOS-1 images, validated by GPS data, allow to characterize and quantify the surface displacements during the monitoring period (2007-2011). We confirm herein the geometry, the characterization and the present quantification of the active Hengchun Fault deformation that act as an active left-lateral transpressive fault. As the Hengchun ridge faces one of the last major earthquake of Taiwan (December 26th 2006, depth: 44 Km, M_L=7.0), it is needed to better constrain the Hengchun Peninsula active tectonics in order if possible to prevent major destructions in the near future.

1 Introduction

The island of Taiwan is the place of the so rapid NW-SE trending oblique Eurasian versus Philippine Sea Plates convergence (e.g. Ho, 1986, 1988). A Southwest propagation of the deformation in Taiwan is proposed by Suppe (1981; 1984). It is confirmed for instance by the continuous GPS measurements that highlight displacements in the Southern Taiwan of about 6

cm y^{-1} (e.g. Yu et al., 1997). This local shortening rate is about the maximum range in the world. We focus herein in the Southern Taiwan area (so called the Hengchun Peninsula), that is geodynamically interpreted as the Taiwan incipient collision zone (Lallemand et al., 2001, Fig.1) which is the transition of the Manila subduction area toward onshore Taiwan collision. The Hengchun Peninsula is situated at the summit of the outcropping onshore Manila accretionnary prism

5 (Malavieille et al., 2002; Chang et al., 2003).

From the geological point of view, it is a complex area, as its lithology is composed of both folded turbiditesas well as the "Kenting Melange" situated close to the Hengchun Fault zone (Fig.1) and composed of highly deformed shales and large blocks of various lithologies. Evidence of this structural complexity are the five different 1/50.000 scale geological maps (Huang et al., 1997, 2006; Chang et al., 2003 and 2009; Zhang et al., 2016) that have been drawn independently and that are

10 geologically incompatible! Two different major fault zones (Hengchun and Kenting Faults) NNW-SSE trending parallels the eastern side of the 15 km long Hengchun valley and had been recognized by previous authors as potentially active (e.g. Huang, et al., 1997, 2006; Chang, et al., 2003, 2009, etc.). As the Hengchun Peninsula is the place of sensitive industries, such as the TAIPOWER Nuclear Power Plant N°3, it is a major concern to better decipher the neotectonics and the active tectonics of the place. Consequently, we address in this paper the localization, and characterization of the deformation of the

15 Hengchun Fault which is the southernmost onshore active fault in Taiwan.

Below, we first focus on the inputs of high resolution Digital Terrain Model (DTM below) and the orthorectified images of the Hengchun Fault Zone acquired from Unmanned Aircraft/Aerial System (UAS). For a terminological point of view, we used herein the UAS acronym that encompasses all the aspects of deploying those aircrafts and which is less restrictive than Unmanned Aircraft/Aerial Vehicle (UAV) that corresponds only to the platform itself. Then following the classical photo-

20 interpretation techniques, we carefully map and interpret the new morphostructures in term of geological mapping, revealing the active tectonic structures. We also benefit from Persistent Scatterers-InSAR results derived from ALOS-1 radar images, that give us the interseismic displacement along the Line of Sight (LOS herein) of the radar through the 2007-2011 period. The latter is validated by two E-W trending precise leveling lines across the Hengchun Fault and a few GPS stations. Finally, the discussion leads us to propose a simple geodynamic and active tectonic model for the Hengchun Fault that fits with all

25 the available data.

2 High resolution Digital Terrain Model (DTM) obtained from UAS

An Unmanned Aircraft System (UAS), commonly known as a drone, is an aircraft without human pilot on board that flies autonomously, and is now been used widely for many aspects because of its convenience, high resolution, etc. (Huang and Chang, 2014; Fernandez Galarreta et al., 2015 ; Giordan et al., 2015 ; Tokarczyk, 2015 ; Bühler et al., 2016; Deffontaines et

30 al., 2016A). The UAS used in this study is a modified version of the already-available Skywalker X8 delta-wing aircraft reinforced by carbon fiber rods and covered partially by Kevlar fiber sheets. The drone is launched by hand, flies and takes photos autonomously, then glides back down to the ground by using a pre-programmed flight plans organized by ground

control system, and controlled by the ground control station and remote controller. The autopilot system used in this study is composed of and modified from the open source APM (Ardupilot Mega 2.6 autopilot) firmware and open source software Mission Planner, transmitted by ground-air XBee telemetry. In order to generate high resolution DTM and mosaic orthorectified images, a total of 3767 photos were gathered by Sony ILCE-QX1 camera mounted on the crafts, during 5 fly

5   missions, for a total coverage area of 33 km^2 with 8 cm Ground Sampling Distance (GSD). The coverage of the adjacent photos is kept at least for 85% overlap and 45% sidelap. The raw images are processed by Contextcapture and Pix4Dmapper software mutually, the data sets generated in this study are orthoimages and DTMs, with a grid spacing of 10 cm. Prior to the morphotectonic analysis (Deffontaines et al., 1991, 1993, 1997, 2016A; Pubellier et al. 1994...), the quality of the data set (see whole data set on figure 2) needs to be evaluated. 18 ground control points are extracted from airborne LiDAR dataset

10   and from the airborne LiDAR associated 25 cm resolution orthorectified image. Most of the ground control points are situated on crossroads, targeted and georeferenced from orthorectified image and elevation from the airborne LiDAR data, respectively. The comparison of the UAS DTM with airborne LiDAR data gives a root-mean-square deviation (RMSD) of 4.1 cm with maximum error of 42.5 cm from 26 sites of open bare ground area, e.g. roads, school playgrounds, unvegetated terrains, and parking lots. The elevation of the check points is averaged from an area of 4 m^2, equal to the grid

15   size of airborne LiDAR data. The distribution of the ground control points and checked points are located on Fig 2b. The Fig. 3 illustrates some case examples of the quality of both the DTM as well as the orthorectified image of the Hengchun Fault. The morphostructures analyses based on photo interpretation are conducted accordingly.

3 Geology of the Hengchun area

From a geologic and geodynamic point of view, the Hengchun Peninsula is interpreted as the northern tip of the Manila

20   accretionnary prism (Malavieille et al., 2002; Chang et al., 2003). It is mainly composed of several lithological formations that are described below from the older to the younger ones (see location on the cross-section of Fig. 1C).

The Mutan Formation is farther the larger outcropping formation of the Hengchun Peninsula. Middle to late Miocene in age, it is composed of classical turbidites deposits such as interbedded sandstones (channels and levees) and shales (Sung and Wang, 1986). The Mutan Formation is a very thick pile (locally several thousands of meters) and highly deformed turbidites

25   (locally even overturned, Chang et al., 2003).

The complex Maanshan formation, late Miocene, Pliocene up to Quaternary in age, is a mix of submarine erosion and depressions fill-in of both Mutan and Kenting formations (Cheng and Haung, 1975; Page and Lan, 1983; Lin and Wang, 2001; Huang, 2006). The Maanshan formation outcrops partly in the South of the Hengchun Basin (CGS geological map (Sung, 1991), see panorama of the Hengchun Basin on Figure 4). We believe that the Maanshan formation composes partly

30   the basement of the Hengchun Basin and the offshore Manila accretionnary prism to the south (Lundberg et al., 1992 and 1997; Reed, et al., 1992).

The Kenting Mélange, which is only outcropping east of the Hengchun Basin, is known as a tectonic Mélange (e.g. Tsan, 1974A and B; Page and Lan, 1983; Huang, 1984; Pelletier and Stephan, 1986; Huang et al., 1997; Chang et al., 2003, 2009A and B; Deffontaines et al., 2016B, Zhang et al., 2016; Malavieille et al., 2016). It is interpreted as a chaotic tectonostratigraphic unit containing blocks of various origin (ophiolitic and sedimentary), size and lithology embedded in a sedimentary matrix (Malavieille et al., 2016). It is herein interpreted as a large tectonic breccia of composite ages that ranges from 1 to 10Ma (see Malavieille et al., 2016) as it mixes various sizes of different blocks and different turbiditic and shale bodies (Page and Lan, 1983; Lin and Wang, 2001, Chang et al., 2003). To our point of view this shaly/blocky tectonic Mélange is injected (intruded) within the major fault zones south of Taiwan due to both the plate convergence and high pressure of fluids at depth (see also Deffontaines et al., 2016B). Future scientific work is needed in order to both precise the processes that creates this tectonic Melange and to reconstruct (or inverse) its evolution through time as there is still different incompatible assumptions and hypotheses (e.g. Malavieille et al., 2016).

Geological mapping in the fields lead us to look for active tectonic cracks within anthropic concrete dykes. They reveal the clear transpressive and thrusting component of the Hengchun Fault (Figure 5). As the concrete dykes are manmade and very recent, it is easy to reconstruct and inverse the deformation following the Angelier's methodology settled along the Longitudinal Valley Fault (see also Lee et al., 1998, 2000, 2001, 2003, 2005, 2006).

From a structural point of view, the Hengchun Fault geological map that we propose (Fig. 6), is the result of (1) field studies (Figs. 4 and 5 taken Jan. 3rd, 2007), (2) the synthesis of previous geological mappings (CPC, 1993, the CGS-Sung, 1991, Chang et al., 2003, Chen et al., 2005, and more recently the Giletycz et al., 2015) ; and (3) a detailed photo-interpretation of both the orthorectified mosaic of the UAS aerial photograph as well as the hill-shading of the high resolution UAS derived DTM (Fig. 5). The detailed structural photo-interpretation of the Hengchun Fault area checked in the fields, takes into account the basic morphostructural principles (Deffontaines et al., 1991, 1993, 1997; Pubellier et al., 1994) such as the geometry of the drainage pattern (bayonet tracks, curves and alignments), the alignments of small scarps present in the flat Hengchun Basin (Fig. 6, index 5) that helps to get the morphotectonic features (Fig. 6, faults that affect the topography, index 2 for instance). We also added on the Hengchun Fault geological mapping, geomorphological objects such as paleo-surfaces (index 5 on Fig.6) which are easily recognized by smooth textures and structures above the Kenting Mélange. Those paleo-surfaces are slightly tilted, folded and uplifted east of the Hengchun Fault and are witnesses of the vertical uplift of the tectonic activity of the Hengchun Fault. Unfortunately, due to the slight tilt, it remains uneasy to extract fold axes from those paleo-surfaces. It should be interesting to date these paleo-surfaces in order to get the middle to long-term activity of the deformation. We select also the chevrons from the morphostructural analysis of the high resolution UAS-DTM (index 6 on Fig. 6). Chevrons correspond to the top of harder rocks tilted structural surfaces within the Kenting Mélange East of the Hengchun Fault. They reveal opposite tilted strata, consequently the presence of folds (anticlines as well as synclines, index 7 on Fig. 6) close and parallel to the Hengchun Fault zone. Some tectonically offset and eroded mud volcanoes are also identified and mapped herein (index 3, on Fig. 6), especially in the South Hengchun Basin and close to the Taipower Nuclear Power Plant N°3. Those situated to the south of the study area were already evidenced by Giletycz (2015). They appear on

the UAS DTM as characteristic "elongated conic volcanic" shape relief above the flat marine and alluvial lowland terrace. There western side are locally affected by landslides (Fig. 6). We interpret these mud volcanoes as the outcropping traces of the shale intrusions within the Hengchun Fault zone very probably due to fluids overpressure at depth in relation to the intense tectonic stress (see also Deffontaines et al., 2016B).

5 The Hengchun Fault is recognized as active (Bonilla, 1976; Hsu and Chang, 1979; Lee, 1999; Lin et al., 2000; Deffontaines et al. 2001). Geological mapping in the field reveals many active cracks within anthropic concrete dykes. These cracks highlight the clear transpressive and thrusting component of the Hengchun Fault (Fig. 5). One may note that we cannot recognize clearly in the topography the trace of the Hengchun Fault as a unique straight line thrusting (see Fig. 6) contrasting to the CGS geological mapping (Sung, 1991) or its sinusoidal shape on the CPC geological mapping (1993). We only

10 highlights herein the Hengchun Fault Zone which is made of locally aligned segments of faults that affect the eastern part of the very recent Hengchun Basin deposits (cf. index 2 on Fig. 6).

The active Hengchun Fault appear on Figure 6 as made of several parallel small aligned straight "faults segment" with a transpressive thrusting component (see Fig. 6, index 2). This is in contrast with the rectilinear drawing of the CGS geological mapping (Sung, 1991) or its sinusoidal shape on the CPC geological mapping (1993). But remember that regional geological

15 maps aim at both stratigraphy and structure where fault trace is putting at where maximum stratigraphic throw locates (or just approximately) which may have large differences with the active fault trace situated strictly at active lines where last rupture locates. Moreover on land, last fault rupture can only be identified by geomorphic features; not by drilling or geophysical prospecting.

From the dating of the deformation point of view, the vertical long-term slip rate has been settled from marine terraces study

20 and estimated of 6.3 mm y^{-1} at Haikou and 3.8~6.1 mm y^{-1} at Nanwan (Chen and Liu, 1993). Other marine terrace studies from WS Chen (CGS reports in Chinese) show similar long-term slip rate. Further datings ought to be undertaken in order to better characterize the ages of the terraces, paleo-surfaces and the different deposits of the Hengchun Basin in order to inverse and reconstruct the tectonic history (Liew and Lin, 1987).

4 Inputs of PS-InSAR interferometry on the Hengchun Fault

25 In order to get the tectonic activity of the Hengchun Fault, we processed 13 radar images (ALOS-1 PALSAR images acquired in L-Band (λ = 23.6 cm)) in ascending mode between January 2007 and January 2011 so providing 4 years of monitoring, through the STaMPS software (Hooper et al. 2007). A series of 12 interferograms has been generated, all with respect to a unique « Super Master » image situated in the mid-time series (Pathier et al., 2003; Fig. 7). The method identifies PS pixels (more than 20.000 PS points are available, see Fig.8A and 8B) that are characterized by their phase

30 stability over the whole period. PS analysis leads us to extract a map of mean LOS surface velocities for each PS and also to catch their displacements through time series. The PS-InSAR base (black and white star) is chosen with the more stable place in the figure (very few displacements - see close to Haikou - north of the Hengchun Valley) within the monitoring time

period. Nevertheless, this location might be submitted to small continuous uplift or small continuous subsidence that may explains local discrepancies with the GPS average annual displacement.

The results (Fig. 8A and 8B) show an impressive density of PS (more than 140 PS/km²) in this area where both human activity and luxuriant vegetation prevail. The PS map reveals a clear continuous difference in LOS velocities across the Hengchun Fault where the Hengchun valley (western side of the Hengchun Fault) is subsiding with values ranging from -5 to -10 mm y^{-1} contrasting with the westernmost Hengchun ridge which is uplifting. The eastern side of the Hengchun Fault is characterized by the rapid increasing uplift of the Kenting Mélange up to a maximum that seems to parallel the Hengchun Fault. Farther east the PS LOS velocities decrease with the distance to the Hengchun Fault so the east of the Hengchun peninsula appears to be slightly tilted. We observe in the Hengchun peninsula a similar dissymmetric active vertical behaviour as in the Coastal Range (Eastern Taiwan) : the western part of the relief is highly actively uplifting and folding contrasting to the eastern part characterized by a decreasing uplifting and which is slightly tilted to the east (see also Deffontaines et al., 2016A). We note in Fig. 9B and Fig. 10, the coherence in between the PS LOS velocities and the GPS measurements (coloured large dots that we put into the same LOS radar geometry). Consequently, those PSInSAR results offer a precise mapping of the active interseismic splays of the Hengchun Fault and allow the quantification of the tectonic displacements.

Dealing with the Kenting Fault, with the data used in this study we see no gradient of PS LOS velocity, nor differential noticeable displacements on the GPS stations situated around the Kenting Fault (see Figure 8A-8B and 9A-9B). Moreover from the geological mapping analysis (Chang et al. 2003), the Kenting Fault has a sinusoidal planimetric geometry that follows more or less the topographic isocontour of the relief. So the Kenting Fault is a low dipping thrust fault. Consequently, this fault may be either locked at the surface, or an inherited inactive fault, or have a tectonic activity that we do not observe on this PS-InSAR dataset.

We note a great coherence in between the PS and the available GPS measurements (colored large dots on fig. 8B) provided on two stations. For comparison purposes, the average annual GPS displacements acquired in the InSAR monitoring time period have been projected on the radar LOS. We compared also these PS results with leveling data acquired during the same period of time (between March 2008 and April 2011, during 3 campaigns of measurement). As for GPS data, we converted vertical leveling measures into InSAR LOS values. Figure 9 allows comparing the leveling data, the mean LOS velocities of PS along the leveling lines, and GPS data for the two stations situated close to the leveling lines. One may note the agreement between all of them. One may note the local heterogeneity of the displacements (e.g. small subsidence as well as small uplift) within the Hengchun valley which is highlited by both the HENC GPS station that gives the absolute uplift displacement and the PS-InSAR data with various coloured dots that range from blue to orange situated on both side of the O value - see the colour scale.

Moreover, in order to better characterize the Hengchun Fault activity, and quantify the LOS velocity variation on both sides of Hengchun Fault, we computed the LOS velocity offset across the fault, using different profiles perpendicular to the fault line. This offset characterizes the slip rate of the fault. We present two specific profiles in Fig. 10 (see location Fig. 8). The

two PS profiles, which run transverse to the Hengchun Fault, one north of the Hengchun valley close to the Checheng city, and the second one southward (close to Hengchun city), show LOS offset less than 10 ± 2.5 mm y^{-1}.

Thanks to a series of more than 30 profiles perpendicular to the fault, we computed the interseismic LOS velocity offset along the fault, from North to South, with values reaching 7 ± 2.5 mm y^{-1} that reveals the clear tectonic activity of the
5   Hengchun Fault (Fig. 11). One may note the excellent coherence between slip rates derived from PS analysis and the GPS measurement (projected in LOS) represented by the yellow triangle, (see Fig. 11). This is a major result from this study as it demonstrates the intersismic activity of the fault, and allows obtaining the average annual interseismic LOS displacement of the Hengchun Fault, and its spatial variation along the fault.

StaMPS gives also access to time series of displacement, from 2007 to 2011. We can thus derive at each image acquisition
10   date the displacement related to the fault (a cumulated slip value), then allowing monitoring its slip variation through time. The time series of slip values (Fig. 12) does not show any clear acceleration, it only expresses a linear behavior of the fault during this period.

5 Discussion: up-dated Hengchun active tectonic model

Many different tectonic models have been proposed on the active Hengchun Fault zone (thrust, left-lateral strike-slip...). But
15   it is needed to give both structural and active tectonic arguments for the Hengchun Fault (e.g. Liew and Lin, 1987; Central Geological Survey and CPC geological mappings -1991and 1993 respectively; Chen and Liu, 1993, 2000; Chang et al., 2003, 2009A and 9B; Chen et al. 2005...).

The simplest model that we propose herein that fits with the oblique NW trending Taiwan geodynamic convergence (Suppe, 1984), the E-W displacements measured by GPS data (Yu et al., 1997), the geological dataset and the geological mapping
20   (CPC-1993 and CGS- Sung, 1991; Chang et al., 2003 and 2009, Giletycz et al., 2015), our detailed UAS DTM photo-interpretation (Fig. 6) and our interferometric 2009-2011 PS LOS displacements (Fig. 8A and 8B), is given for the western part of the onshore Hengchun Peninsula (Fig. 13).

From the interferometric point of view, if we generalize, the western Hengchun Peninsula is slowly uplifting toward the LOS (less than +1 cm y^{-1}) contrasting to the slow subsidence of the eastern part of the Hengchun Peninsula (-0.25 cm y^{-1}). So as
25   the average displacements deduced from PS-InSAR across the Hengchun Fault is continuous across the fault zone, it shows the existence of a clear interseismic creeping component, with a value of 0.8 mm y^{-1} along the LOS. The variation of displacements on both sides of the Hengchun Fault zone reveals also the progressive folding of the Hengchun Fault zone: the eastern hanging wall is progressively uplifting contrasting to the progressive subsidence of the Hengchun Basin (Foot Wall - see Fig. 9 and 10). These interferometric results combined with the structural photo-interpretation (Fig. 6) show that the fault
30   is only locally outcropping and that active folding occurs at depth, increasing progressively with time stress and strain at depth.

Consequently due to the structural geometry, the Hengchun Fault appears to act as an active left lateral transpressive strike-slip fault with an active uplifting and folding (anticline) of its eastern hanging wall, contrasting to the active subsidence of the western footwall (which corresponds to the easternmost part of the Hengchun Basin). Moreover the Hengchun Fault is not outcropping along one continuous North to South small straight line but describe a "Fault Zone" made of little active fault segments (see Fig. 6). One may note that the left lateral strike-slip motion has been deduced from the obliquity of the GPS arrows evidenced in the bibliography (e.g. Chang et al., 2003). Therefore the figure 13 shows a simple model where the Hengchun Fault acts as a transpressive left-lateral N160°E trending fault zone. Its active hanging wall is overthrusting and is actively folding the topographic surface that tilts and folds the paleo-surfaces, and marine terraces. The Hengchun Basin (Hengchun Fault footwall - and west of it) under the transpression is folded as well, and is actively subsiding with a parallel to the fault syncline axis that helps for the lagoonal deposition of the Pleistocene/Holocene Hengchun Basin deposits (Chen et al., 1991).

Many faults in Taiwan (e.g. Chelungpu Fault - 921 Chichi Earthquake, September 21st, 1999) present both component of slip (left-lateral strike-slip and thrusting) such as the Hengchun Fault. Dealing with the amplitude of the Hengchun Fault deformation, the interferometric displacement toward the LOS (0.8 ± 0.2 cm y^{-1}) correspond to the instantaneous interseismic slip rate that could be a bit different than the vertical long term slip rate deduced from the marine terraces datings 6.3 mm y^{-1} at Haikou and 3.8~6.1 mm y^{-1} at Nanwan (Chen and Liu, 1993). From this slight difference in between the long term and the instantaneous slip rates, we may deduce the fact that the Hengchun Fault may be not only a creeping fault.

6 Conclusions and perspectives

First, dealing with the technical and methodological conclusions, the flights of UAS with image acquisition lead us capable to produce through photogrammetry. A high resolution DTM of the Hengchun Fault area with a less than 7 cm ground resolution and less than 40 cm precision is then produced for this study. However for some places, the texture may change rate quicker and higher than the image capture acquisition, like for example the lakes or water surfaces due to sunlight reflection for instance, which causes noises in DTMs. Concerning the DTM photo-interpretation, especially for the active geological structures, the terrain is easily to be modified by human activity in Taiwan: cities and farmer land are rapidly growing in some areas concealing morphotectonic structures. Fortunately, the ortho-mosaic images help to recognize those artefacts. Overall, the autonomous UAS and well developed photogrammetry technique allow generating conveniently high detail topographic information, and help to carry on long term scale morphotectonic study. Integrating of PS-InSAR data giving the short term active movement of the Hengchun Fault and High Resolution DTM structural photo-interpretation acquired from UAS demonstrates longer term topographic deformations and anomalies, thus providing one of different tectonic deformation to locate, characterize and quantify the active tectonics features.

Then with these so useful high resolution topographic data, we undertook a classical geological and geomorphological photo-interpretation that lead us to up-date and refine the pre-existing CPC-1993 and CGS-1991 geological maps, especially on both side of the Hengchun Fault. The latter lead us to precise the structural geometry of the Hengchun Fault in the Peninsula (Fig. 6). Moreover, the PS-InSAR interferometric processing that we carried out over the Hengchun Peninsula

5 from 2007 to 2011 with more than 12 coherent interferograms reveal clear interseismic displacements of the Hengchun Fault. Moreover, our interferometric results are in agreement with GPS data and reveal the active section and folding of the eastern hanging-wall of the Hengchun Fault of about 0.8 ± 0.2 cm y^{-1} toward the LOS. Furthermore the footwall is submitted also to a complementary active subsidence related to the development of an active syncline parallel to the Hengchun Fault. These displacements are a cumulative vector taking into account both planimetric and vertical components of the deformation. Our

10 results are fully coherent with both two leveling lines E-W trending across the Hengchun Fault and three continuous GPS stations. Moreover PS density (more than 140 PS Km^{-2}) offers a spatial density of measurements that is greatly higher than that the one offered by GPS, allowing us a global and whole coverage and mapping of the active Hengchun Fault deformations.

Moreover PS density (more than 140 PS/km²) offers a spatial density of measurements that is greatly higher than that the one

15 offered by the GPS, allowing us a global and whole coverage and mapping of the active Hengchun Fault deformations.

From the active tectonics conclusions, we deduce that the highly dipping Hengchun Fault acts as an inter-seismic creeping left-lateral strike-slip fault with a clear transpressive component of 0.8 cm y^{-1} in LOS that is associated with active foldings. As the PS interferogram spectrum increase continuously from W to E above the whole Hengchun Fault zone, it means that the Hengchun Fault is actively folding at depth. Moreover, the lack of clear PS discontinuity across the Hengchun Fault zone

20 proves that it is not offsetting the topography (and outcropping) during the acquisition monitoring period (2007-2011). This signs the slow continuous increase of tectonic stress at depth which is a major clue for a future earthquake in that area.

Unfortunately, the active differential displacement on both side of the Kenting Fault is much more difficult to highlight with our PS results, due (1) to the low dipping of that fault deduce from its mapping geometry, or (2) to an inherited inactive fault, or (3) a locked fault at the surface, and also maybe due to (4) the ductile rheology of the underlying formation (Mutan clay

25 turbidites - MT). Consequently, it is needed to much better map the Kenting Fault in order to better understand its rheology and active behaviour (work under progress).

Anyway, the shallow seismicity (Deffontaines et al., 2016B) confirms the high onshore shallow tectonic activity that hits the Hengchun Peninsula. The deep offshore major Hengchun earthquake (December 26th 2006, depth: 44 Km, M_L=7.0) also participated to the active deformation of the Peninsula.

30 Finally, due to the homogenous 0.8 cm y^{-1} LOS displacement toward the LOS all along the 15 Km of the Hengchun Fault studied area, it is definitely needed to better constrain the Hengchun peninsula active tectonics in order to prevent major destructions and major failure in the near future as for example for the present so sensitive energy industries (e.g. the Taiwan Nuclear Power Plant N°3 situated along the southern tip of the Hengchun Fault).

7 Acknowledgements

We are grateful to Andy Hooper for having developed and permitting to use the 'StaMPS/MTI' algorithms, and the constructive remarks of both reviewers that help to improve significantly the manuscript. We thank also the Japan Aerospace Exploration Agency (JAXA) for the ALOS 1 data in the scope of PI 112-0001 project (project number: 5226904000 PI: Benoit Deffontaines. This project was partially supported by the LIA ADEPT (now D3E), N°536 French CNRS-NSC (now MOST), and Taiwan MOST 105-2116-M-027-003.

References

Bonilla, M.G.: Summary of Quaternary faulting and elevation changes in Taiwan: Mem. Geol. Soc. China, 2, 43-55, 1976.

Bühler, Y., Adams, M.S. Bösch, R., and Stoffel A.: Mapping snow depth in alpine terrain with unmanned aerial systems (UASs): potential and limitations, The Cryosphere, 10, 1075–1088. doi:10.5194/tc-10-1075-2016, 2016.

Chang, C. P., Angelier, J., Lee, T. G., and Huang, C.: From continental margin extension to collision orogen: structural development and tectonic rotation of the Hengchun peninsula, southern Taiwan, Tectonophysics, 361, 61–82, 2003.

Chang C.P., Angelier, J., and Lu, C.Y.: Polyphase deformation in a newly emerged accretionary prism: Folding, faulting and rotation in the southern Taiwan mountain range, Tectonophysics , 466, 395–408, 2009A.

Chang C.P., Angelier J., Huang C.Y.: Evolution of subductions indicated by Mélanges in Taiwan, in S.Lallemand and F. Funiciello (eds), Subduction Zonz Geodynamics, DOI 10.1007/978-3-540-87974-9, Springer-Verlag Berlin Heidelberg, pp.: 207-225. 2009B

Chen, H. W., Wu, L.C., Huang C.Y., and Koichiro, M.: Late Pleistocene molluscan paleoecology of lagoon deposits of the Szekou Formation, Hengchun Peninsula, Southern Taiwan, Proceedings of the Geological Society of China, 34, 1, 57-87. 1991.

Chen, W. S., Lee, W. C., Hunag, N. W., Yen, I. C., Yang, C. C., Yang, H. C., Chen, Y. C., and Sung, S. H.: Characteristics of accretionary prism of Hengchun Peninsula, southern Taiwan: Holocene activity of the Hengchun Fault, Western Pacific Earth Sciences, 5, 129-154, 2005.

Chen, Y. G. and Liu, T. K.: Holocene radiocarbon dates in Hengchun Peninsula and their neotectonic implications, Journal of the Geological Society of China, 36, 4, 457-479, 1993.

Chen, Y. G. and Liu, T. K.: Holocene uplift and subsidence along an active tectonic margin south-western Taiwan, Quaternary Science Review, 19, 9, 923–930, 2000.

Cheng, Y. M. and Huang, C. Y.: Biostratigraphic study in the west Hengchun Hill, Acta Geologica Taiwanica, 18, 49-59, 1975.

Chinese Petroleum Corporation (CPC): Geologic map of Taiwan, 1:100,000, No 7, Kaohsiung-Pingtung, Prepared by the Chinese Petroleum Corporation, Printed by the Chinese Society of Survey Engineering, 1993.

Cigna, F., Del Ventisette, C., Liguori, V., and Casagli N.: Advanced radar-interpretation of InSAR time series for mapping and characterization of geological processes. Nat. Hazards Earth Syst. Sci., 11, 865–881, 2011.

Deffontaines, B. and Chorowicz, J.: Principle of drainage basin analysis from multisource data, Application to the structural analysis of the Zaire Basin, Tectonophysics, 194, 237-263, 1991.

5   Deffontaines, B., Pubellier, M., Rangin, C., and Quebral, R.: Discovery of an Intra-arc transform zone in Mindanao (Philippines) using morphotectonic data, Zeistchrift für Geomorphologie, Berlin - Stuttgart., Suppl.-Bd. 94, 261-273, 1993.

Deffontaines, B., Lee, J.C., Angelier, J., Carvalho, J., and Rudant, J.P.: New geomorphic data on Taiwan active orogen: a multisource approach, Journal Geophysical Research, 99, B8: 20,243-20,266, 1994.

Deffontaines, B., Lacombe, O., Angelie,r J., Chu ,H. T., Mouthereau, F., Lee, C. T., Deramond, J., Lee, J.F., Yu, M. S., and
10   Liew, P. M.: Quaternary transfer faulting in Taiwan Foothills: Evidence from a multisource approach, Tectonophysics, 274, 1-3, 61-82, 1997.

Deffontaines, B., Chang, K. J., Champenois, J., Fruneau, B., Pathier, E., Hu, J.C., Lu, S. T., and Liu, Y. C.: Active interseismic shallow deformation of the Pingting terraces (Longitudinal Valley – Eastern Taiwan) from UAV high-resolution topographic data combined with InSAR time series, Geomatics, Natural Hazards and Risk, 1-18,
15   http://dx.doi.org/10.1080/19475705.2016.1181678, 2016A.

Deffontaines, B., Liu, C.S., and Hsu, H.-H.: Structure and deformation of the Southern Taiwan accretionary prism: The active submarine Fangliao Fault Zone offshore west Hengchun Peninsula, Tectonophysics, 692, 227–240, http://dx.doi.org/10.1016/j.tecto.2016.11.007, 2016B.

Galarreta, J. F., Kerle, N., and Gerke, M.: UAV-based urban structural damage assessment using object-based image
20   analysis and semantic reasoning, Nat. Hazards Earth Syst. Sci., 15, 1087–1101, 2015.

Giordan D., Manconi, A., Facello, A., Baldo, M., dell'Anese, F., Allasia, P., and Dutto, F.: Brief Communication: The use of an unmanned aerial vehicle in a rockfall emergency scenario, Nat. Hazards Earth Syst. Sci., 15, 163-169, 2015.

Giletycz, S.: Landscape dynamics of the Hengchun Peninsula, Southern Taiwan. PhD dissertation, National Central University, Chungli, Taiwan. 184p. 2015.

25   Giletycz S., Loget, N. Chang, C. P., and Moutherau, F.: Transient fluvial landscape and preservation of low-relief terrains in an emerging orogen: example from Hengchun Peninsula, Taiwan, Geomorphology, 231, 169-181, 2015.

Ho, C.S.: A synthesis of geological evolution of Taiwan. Tectonophysics. 125, 1-16, 1986.

Ho, C.S.: An introduction to the geology of Taiwan and explanatory text of the geologic map of Taiwan. Taipei, Taiwan, Central Geological Survey, Ministry of Economic Affairs, 192p. 1988

30   Hooper, A., Segall, P., Zebker, H.: Persistent scatterer InSAR for crustal deformation analysis, with application to Volcán Alcedo, Galapagos, J. Geophys. Res, 112, B07407, doi: 10.1029/2006JB004763. 2007.

Hooper, A.: StaMPS/MTI Manual, version 3.1. Delft Institute of Earth Observation and Space Systems Delft University of Technology, The Netherlands. 2009.

Huang, C.Y.: Some planktic foraminifers from the olistostromes of the Kenting Formation, southern Hengchun Peninsula. Acta Geol. Taiwan. 22, 22-34, 1984.

Hsu, T.L. and Chang, H.C. Quaternary faulting in Taiwan: Mem. Geol. Soc.China. 3,155-165, 1979.

Huang, C. Y., Wu, W. Y., Chang, C. P. Tsao, S., Yuan, P. B., Lin, C. W., and Xia, K. Y.: Tectonic evolution of accretionary prism in the arc-continent collision terrane of Taiwan, Tectonophysics, 281, 31-51. 1997.

Huang, C. Y.: Foraminiferal paleoecology of a late Pleistocene lagoonal sequence of the Szekou formation in the Hengchun Peninsula, Southern Taiwan, Proceedings of the geological society of China, 33, 181-206, 2006.

Huang, M. J. and Chang, K. J.: Unmanned Aerial Vehicle (UAV) associated DTM quality evaluation and application. Mag. Chinese Inst. Civil Hydraulic Eng., 41, 4, 52-58. 2014. (in Chinese with English abstract).

Lallemand, S., Font, Y., Bijwaard, H., and Kao, H.: New insights on 3-D plates interaction near Taiwan from tomography and tectonic implications, Tectonophysics, 335, 229-253, 2001.

Lee, C.T.: Neotectonics and active fault in Taiwan, Proceedings of 1999 Workshop on Disaster Prevention/Management & Green Technology, Foster City, CA, USA, 61-74, 1999.

Lee, J.C., Angelier, J., Chu, H.T., Yu, S.B., and Hu, J.C.: Plate-boundary strain partitioning along the sinistral collision suture of the Philippine and Eurasian plates: analysis of geodetic data and geological observation in southeastern Taiwan. Tectonics, 17, 159–181, 1998.

Lee, J.C., Jeng, F.S., Chu, H. T., Angelier, J., and Hu, J.C.: A rod-type creepmeter for measurement of displacement in active fault zone. Earth Planets Space 52, 321–328, 2000.

Lee, J.C., Angelier, J., Chu, H.T., Hu, J.C., and Jeng, F.S.: Continuous monitoring of an active fault in a plate suture zone: a creepmeter study of the Chihshang Fault, eastern Taiwan. Tectonophysics 333, 219–240, 2001.

Lee, J.C., Angelier, J., Chu, H.T., Hu, J.C., Jeng, F.S., and Rau, R.J.: Active fault creep variations at Chihshang, Taiwan, revealed by creep meter monitoring, 1998–2001. J. Geophys. Res. Solid Earth, 108, 21, 2003.

Lee, J.C., Angelier, J., Chu, H.T., Hu, J.C., Jeng, F.S.: Monitoring active fault creep as a tool in seismic hazard mitigation. Insights from creepmeter study at Chihshang, Taiwan. Compt. Rendus Geosci. 337, 1200–1207, 2005.

Lee, J.C., Chu, H.T., Angelier, J., Hu, J.C., Chen, H.Y., and Yu, S.B.: Quantitative analysis of surface coseismic faulting and postseismic creep accompanying the 2003, Mw = 6.5, Chengkung earthquake in eastern Taiwan. J. Geophys. Res. Solid Earth, 111, 21, 2006.

Liew, P. M. and Lin, C. F.: Holocene tectonic activity of the Hengchun Peninsula as evidenced by the deformation of marine terraces, Memoir of the Geological Society of China, 9, 241-259, 1987.

Lin, A. T., Yao, B., Hsu, S. K., Liu, C. S., and Huang, C.Y.: Tectonic features of the incipient arc-continent collision zone of Taiwan: Implications for seismicity, Tectonophysics, 479, 28-42, 2008.

Lin, C.W., Chang, H.C., Lu, S.T., Shih, T.S. and Huang, W.J.: An introduction to the active faults of Taiwan-Explanatory text of the active fault map of Taiwan: Spec. Central Geol. Sury., 13, 122p. 2000. (in Chinese with English abstract)

Lin, S. B. and Wang, Y. R.: Clay minerals in the rock formations on the Hengchun Peninsula, Southern Taiwan, and their tectonic implications, Eastern Pacific Earth Sciences, 1, 2, 157-174, 2001.

Lundberg, N., Reed, D.L., Liu, C. S., and Lieske J. J.: Structural controls on orogenic sedimentation, submarine Taiwan collision. Acta Geologica Taiwanica, 30, 131–140. 1992

5   Lundberg, N., Reed, D.L., Liu, C. S., and Lieske J. J.: Forearc-basin closure and arc accretion in the submarine suture zone south of Taiwan. Tectonophysics, 274, 5–23, 1997.

Malavieille, J., Lallemand, S.E., Dominguez, S., Deschamps, A., Lu, C.-Y., Liu, C.-S., Schnurle, P., and ACT Scientific Crew: Arc-continent collision in Taiwan. New marine observations and tectonic evolution. In: Byrne, T.B. & Liu, C.-S., (Eds.), Geology and Geophysics of an Arc-Continent collision, Taiwan, Republic of China. Boulder, Colorado, Geological

10 Society of America Special Paper, 358, 187-211, 2002.

Malavieille, J., Mollic, G., Gentia, M., Dominguez, S., Beyssac, O., Taboada, A., Vitale-Brovaroned, A., Lu, C.-Y., Chen, C.-T.: Formation of ophiolite-bearing tectono-sedimentary mélanges inaccretionary wedges by gravity driven submarine erosion: Insightsfrom analogue models and case studies, Journal of Geodynamics, 100, pp.: 87-103, http://dx.doi.org/10.1016/j.jog.2016.05.008, 2016

15 Page, B. M. and Lan, C. Y.: The Kenting mélange and its record of tectonic events. Memoir of the Geological Society of China, 5, 227-248, 1983.

Pathier, E., Fruneau, B., Deffontaines, B., Angelier, J. Chang, C. P., Yu, S.B., Lee, C.T.: Coseismic displacements of the footwall of the Chelungpu fault caused by the 1999, Taiwan, Chi-Chi earthquake from InSAR and GPS data, Earth Planetary Science Letters, 212, 73-88. , 2003.

20 Pelletier, B. and Stephan, J. F.: Middle Miocene obduction and late Miocene beginning of collision registered in the Hengchun Peninsula: Geodynamics implications for the evolution of Taiwan, Memoir of the Geological Society of China, 7, 301-324, 1986.

Pubellier, M., Deffontaines, B., Quebral, R., and Rangin, C.: Drainage network analysis and tectonics of Mindanao, Southern Philippines, Geomorphology, 9, 325-342, 1994.

25 Reed, D. L., Lundberg, N., Liu, C. S., and Kuo, B.-Y.: Structural relations along the margins of the offshore Taiwan accretionary wedge; implication for accretion and crustal kinematics. Acta Geologica Taiwanica, 30, 105–122, 1992.

Sung, Q. C. and Wang, Y.: Sedimentary environments of the Miocene sediments in the Hengchun Peninsula and their tectonic implication, Memoir of the Geological Society of China, 7, 325-340, 1986.

Sung, Q.C.: Explanatory text of the geologic map of Taiwan, 1:50000, sheet 69-72, Hengchun Peninsula, Published by the

30 Central Geological Survey, Ministry of Economics Affaires, 77p., 1991. (in Chinese).

Suppe, J.: Mechanics of mountain building in Taiwan. Memo. Geol. Soc. China, 4, 67-89, 1981.

Suppe, J.: Kinematics of arc-continent collision, flipping of subduction, and back arc spreading near Taiwan, Geological Society of China, Mem. 6, 21-33, 1984

Tokarczyk, P., Leitao, J. P., Rieckermann, J., Schindler, K., and Blumensaat, F.: High-quality observation of surface imperviousness for urban runoff modelling using UAV imagery, Hydrol. Earth Syst. Sci., 19, 4215–4228, 2015.

Yu, S.B., Chen, H.Y., and Kuo, L.C.: Velocity field of GPS stations in the Taiwan area. Tectonophysics 274, 41– 59, 1997.

Zhang, X., Cawood, P.A., Huang, C.Y., Wang, Y., Yan, Y., Santosh M., Chen, W., and Yu, M.: From convergent plate margin to arc-continent collision: Formation of the Kenting Mélange, Southern Taiwan, Gondwana Research, 38, 171-182, 2016.
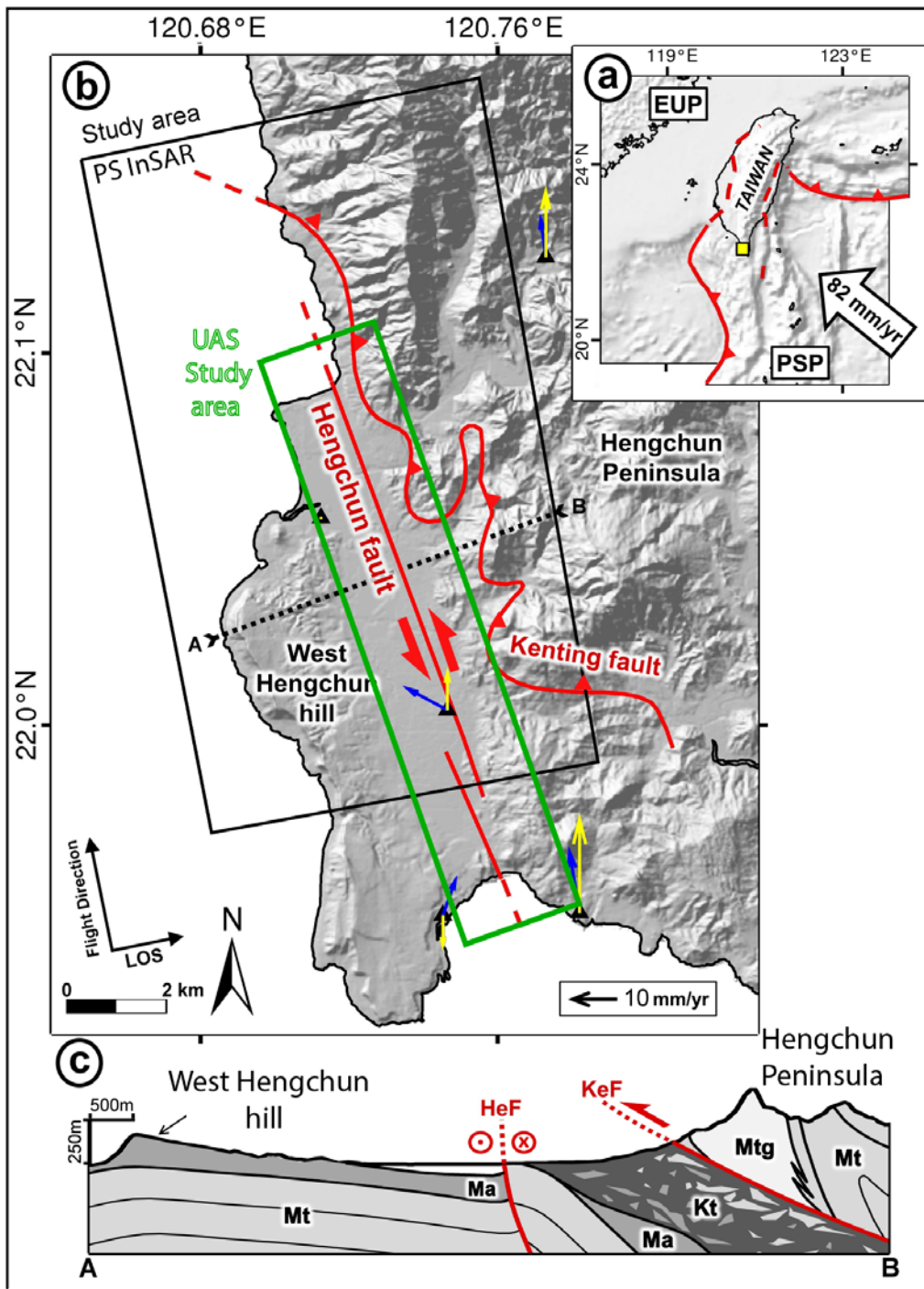
Figure 1: Location of the Hengchun and Kenting Faults within Southern Taiwan. Fig. 1a: Location of the Hengchun Peninsula (yellow quadrangle); EUP Eurasian Plate; PSP: Philippine Sea Plate. 82 mm y[-1] is the rate convergence of the Philippine Sea Plate toward Eurasia (Yu, et al. 1997). Fig.1b: W Hengchun Peninsula hill-shade from the 40m ground resolution DTM: The heavy red lines are Hengchun and Kenting Faults. Black Triangle: used GPS stations; Blue and yellow arrows represent horizontal and

vertical GPS displacements respectively; Black quadrangle study area; A-B location of Fig.1c geological cross-section; Fig. 1c: W-E trending synthetic geological cross-section (modified from Chang et al., 2009B; and Zhang et al., 2016), Ma: Maanshan formation, Mt and Mtg: different facies of Mutan formation, Kt: Kenting Melange, HeF: Hengchun Fault, KeF: Kenting Fault.
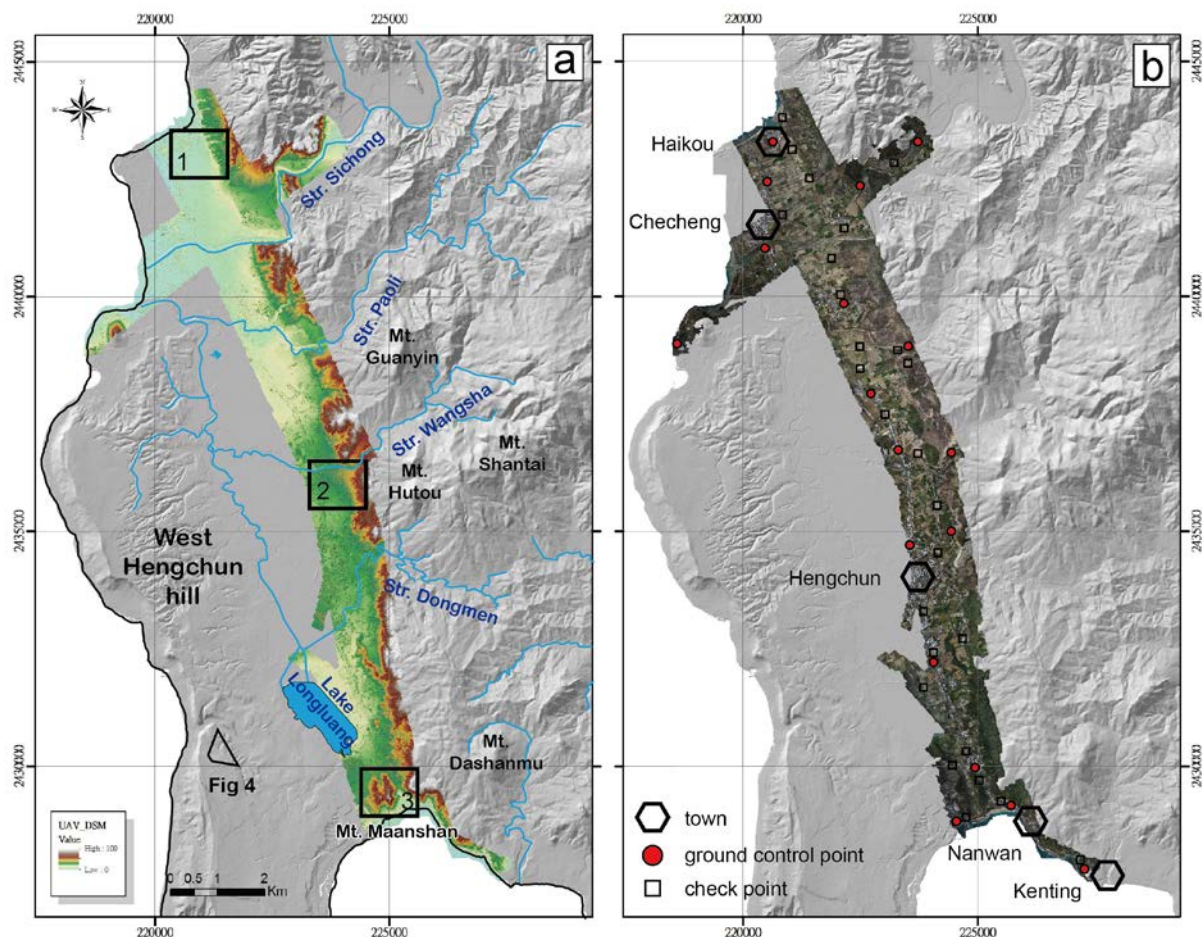
Figure 2: UAS Digital Terrain Model (DTM) and mosaic of orthorectified images, indicate, Fig. 2a and Fig. 2b, respectively. The black hexagons, red circles and rectangles locate cities, ground control points and check points, respectively. One may notice the contrasting relief on both sides of the Hengchun valley: its western flank is a homogenous structural surface slightly dipping east contrasting to the highly eroded eastern part. For both Fig. 2a and 2b, the black and white hill-shade DTM correspond to a part of the 5m ground resolution Taiwan DTM.
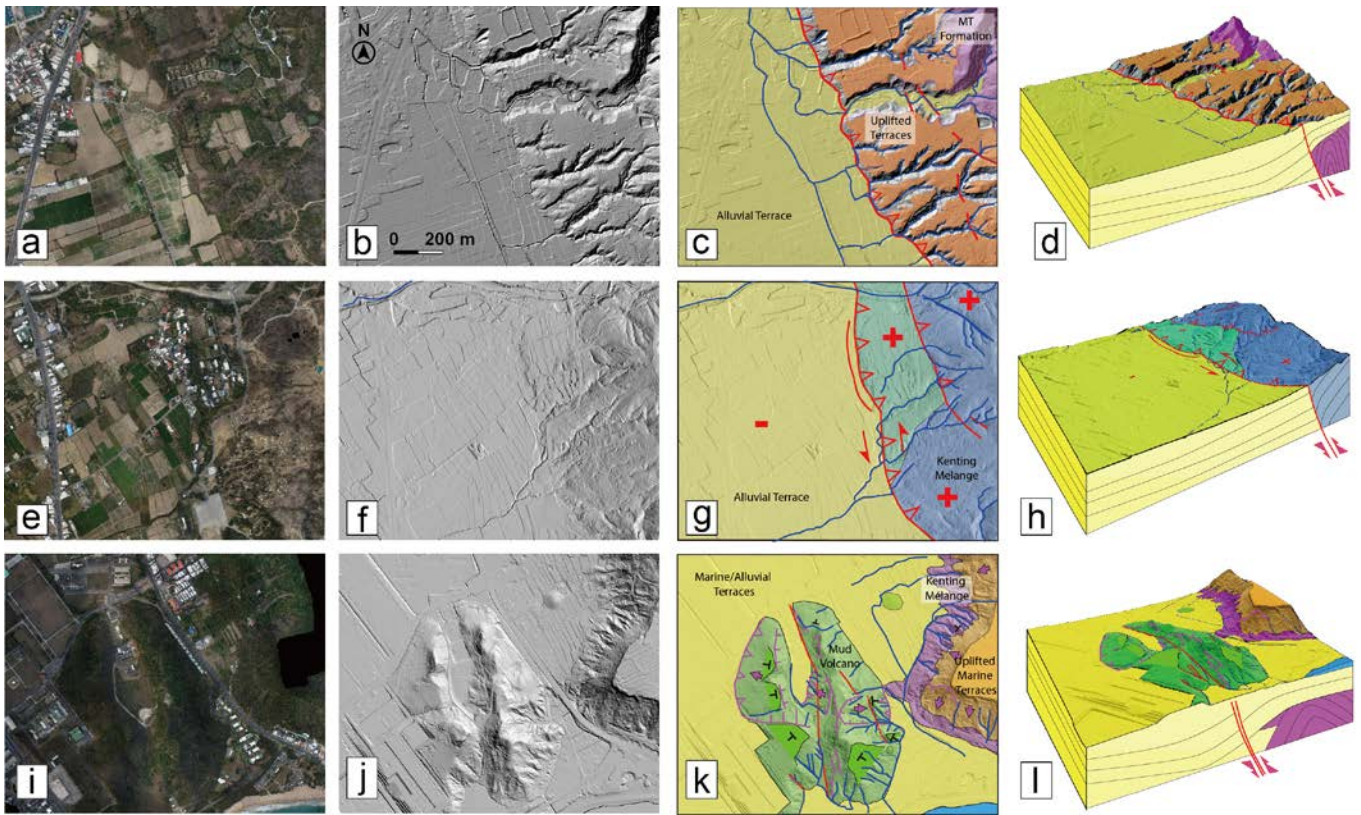
Figure 3: Three case examples taken from North to South of the Hengchun UAS Digital Terrain Model (DTM). Each box cover the same area (1.3 km x 1.1 km): First column (a, e, i) : mosaic of the georeferenced aerial photographs (orthophoto) of each study area. Second column (b, f, j) : Black and white hill-shading relief from UAS derived DTM; Third column (c, g, k): geological map
5   **from the high resolution hill-shade DTM where heavy red line corresponds to the Hengchun Fault, blue line to the drainage, in light yellow : quaternary alluvial and marine terraces, in purple/ light blue due to the DTM transparency the Kenting Melange, in brown the uplifted marine terraces, in light green Mud-volcano and dark green its associated structural surface (chevrons with radial outward dips in black line), purple lines boundaries of landslides ; + : uplifted area; - : subsiding areas, NPP: Taiwan Nuclear Power Plant N°3, MV: Mud volcano; Fourth column (d, h, l) : 3D geological mapping with their associated geological**
10   **cross-sections that shows the Hengchun Fault at depth (red arrows : active fault displacements). blue lines : rivers,** The first line of images highlights the active tectonic scarp of the Hengchun Fault which differentiate 2 blocks: an uplifted (+) locally eroded terraces to the east and a flat lowland sedimentation area to the west. The second line of images highlights the left lateral offset geometry (red arrows) of tributaries (blue line) on a glacis which is uplifted (+) on the east of the Hengchun Fault. The third line of images shows a deformed N-S trending elongated mud volcano (MV) **previously evidenced by Gilevytcz, 2015 in its PhD**
15   **dissertation) situated** close to the Taiwan Nuclear Power Plant N° 3 (NPP and see infrastructures on the lower left corner of the deformed mud volcano) and a flat uplifted (+) terraces (paleosurface of Fig. 6) on the **western side of the captions.**
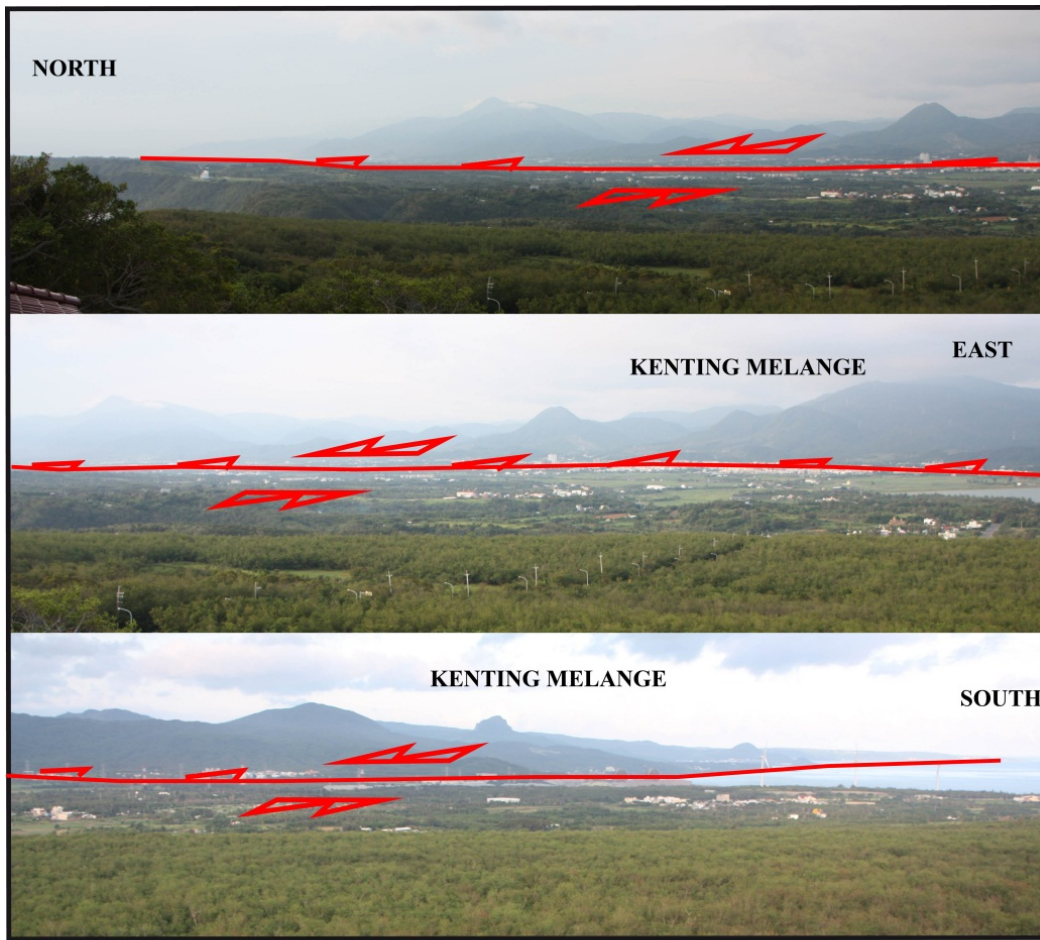
Figure 4: Panorama of the Hengchun Fault observed from the SW part of the studied area. Red lines (1) correspond to the left lateral compressive Hengchun Fault. Note the isolated summits within the Kenting Melange that is composed of highly deformed shales with various huge blocks (olistoliths?) interpreted herein as a tectonic breccia. The location and the direction of the photos where it were taken are indicated on Fig 2a.

Figure 5: Field work photograph of compressive features affecting recent concrete dykes after the Hengchun earthquake (Dec. 26th 2006, M_L=7.0), see location on Fig. 1 near the Fang-Shan village (22.26°N, 120.66°E). The red compass gives the scale of the outcropping deformation (20cm). Thrust associated with three back-thrusts highlighting a small pop-up (below the compass). The
5 **red arrow reveals the thrusting component that affects the new concrete dykes**
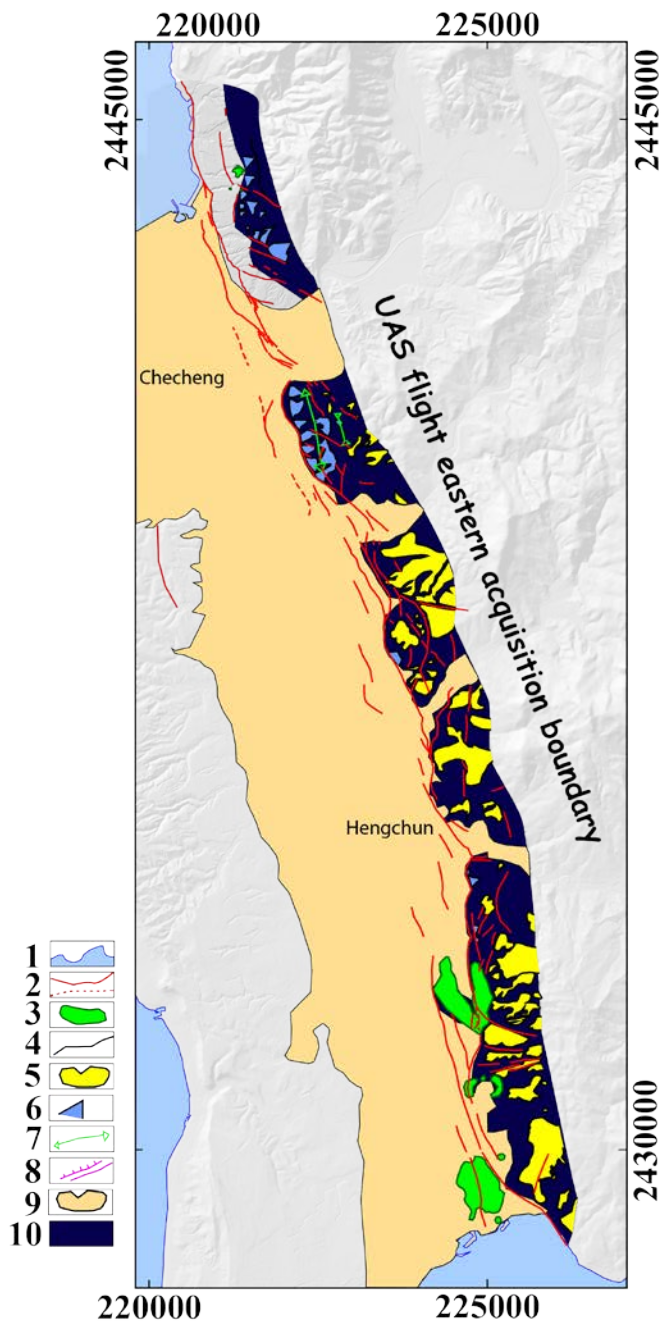
Figure 6: Morphostructural map of the Hengchun Fault: 1. Shoreline; 2. Faults (red lines: certain faults, red dashed lines: inferred); 3: Mud-volcano; 4: Lithological boundaries; 5: Paleo-surfaces; 6: Chevron corresponding to tilted structural surface, 7: Fold axes; 8: Landslide and extrados faults (see Deffontaines et al., 2016B); 9: Hengchun valley alluvial and marine deposits; 10: Kenting Mélange. Note that the Hengchun Fault is made of numerous small parallel faults affecting a rather wide area of the eastern Hengchun valley. It is associated with a N-S trending fold close to Checheng. Some folds that tilt paleosurfaces and NE-SW, E-W and NW-SE oblique faults affect the Kenting Mélange.
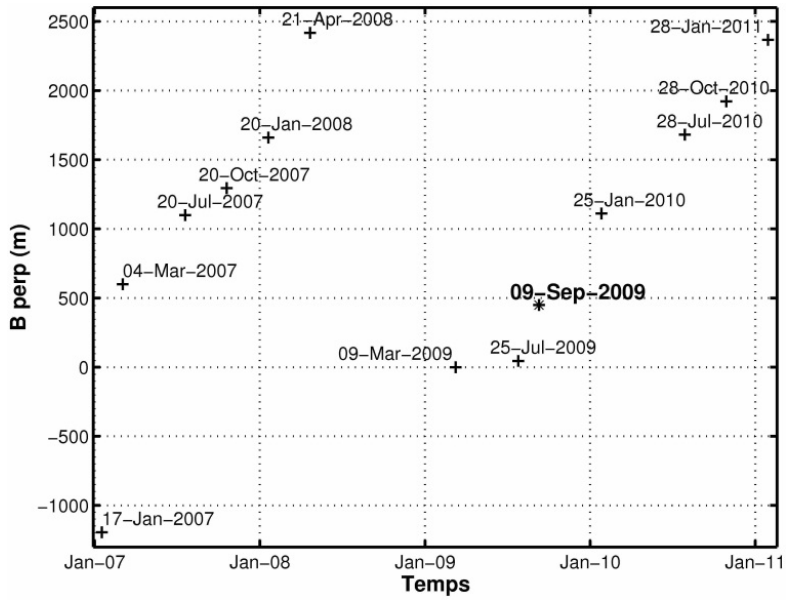
Figure 7: Available ALOS-1 SAR images and their associated perpendicular baselines. All slave images are linked to the best master image chosen in the middle of the time series that maximizes the sum correlation of all intererograms (Hooper et al., 2007).
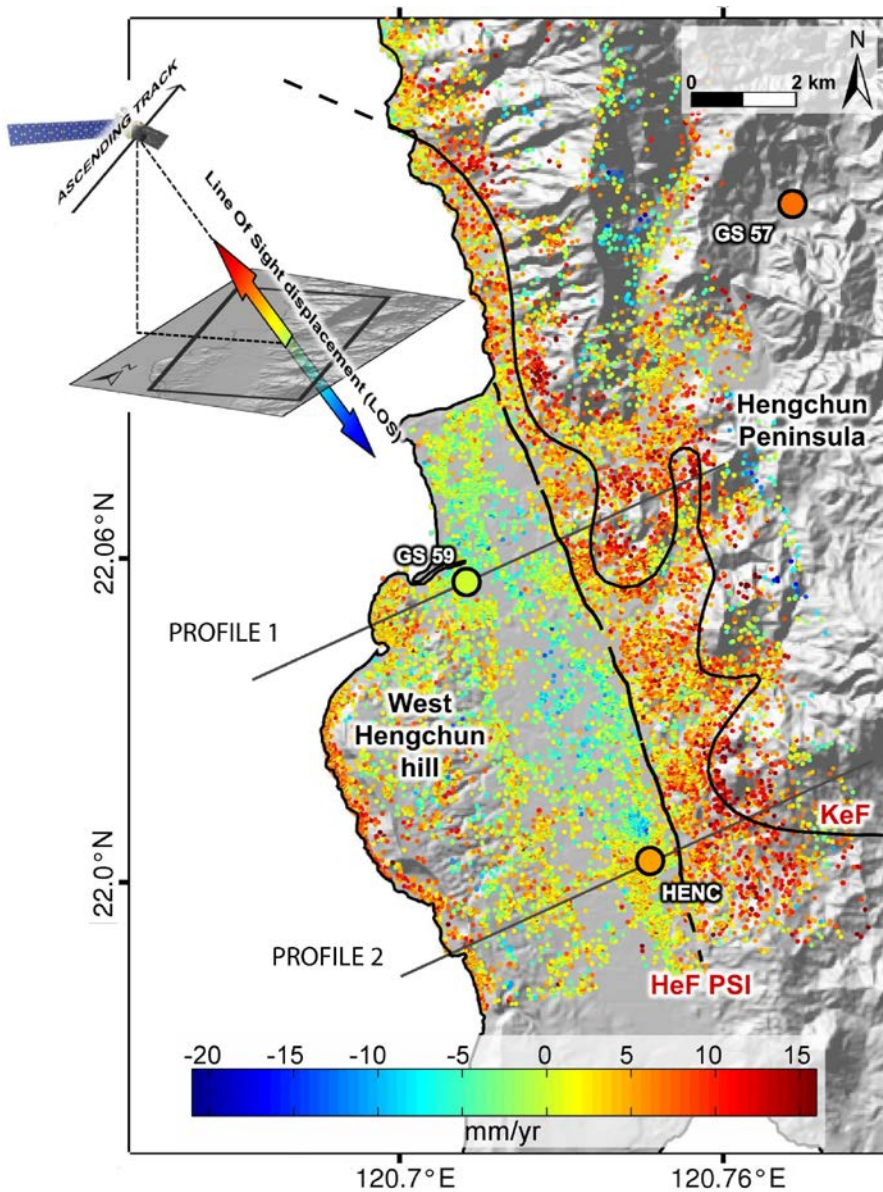
Figure 8: Mean LOS velocities of PSinSAR between Jan. 2007 and Jan. 2011, superimposed to the shaded 40m ground resolution S. Taiwan Digital Terrain Model. **The large black circles are the used GPS points and the color in the circles indicates their average LOS velocity component during the monitoring time period. The black and white star (situated close to Haikou - see location on Fig. 2) correspond to the PSinSAR base.** Black and grey arrows give their horizontal and vertical velocity. Red line: Hengchun Fault. Location of profiles 1 and 2 (see Fig. 10). **One may note the active surrection and folding east of the Hengchun Fault contrasting with the subsidence of its western part (Hengchun valley)**
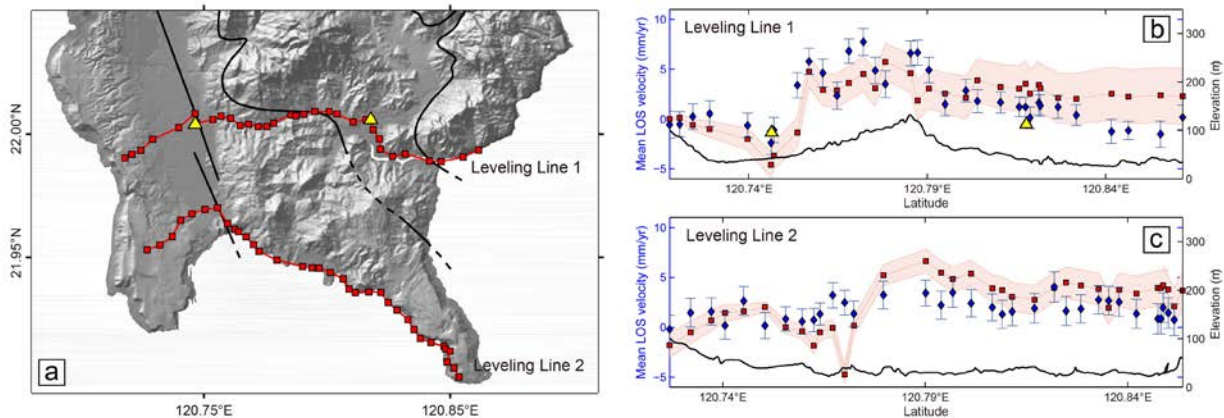
Figure 9a: Location of the leveling lines on the Hengchun Peninsula. Fig. 9b and 9c: associated PS mean velocity with error bars (blue dots,) leveling data (red square and in pink: error bar) and GPS stations data (yellow triangle), projected on LOS. Note the general agreement of all topographic displacement values.
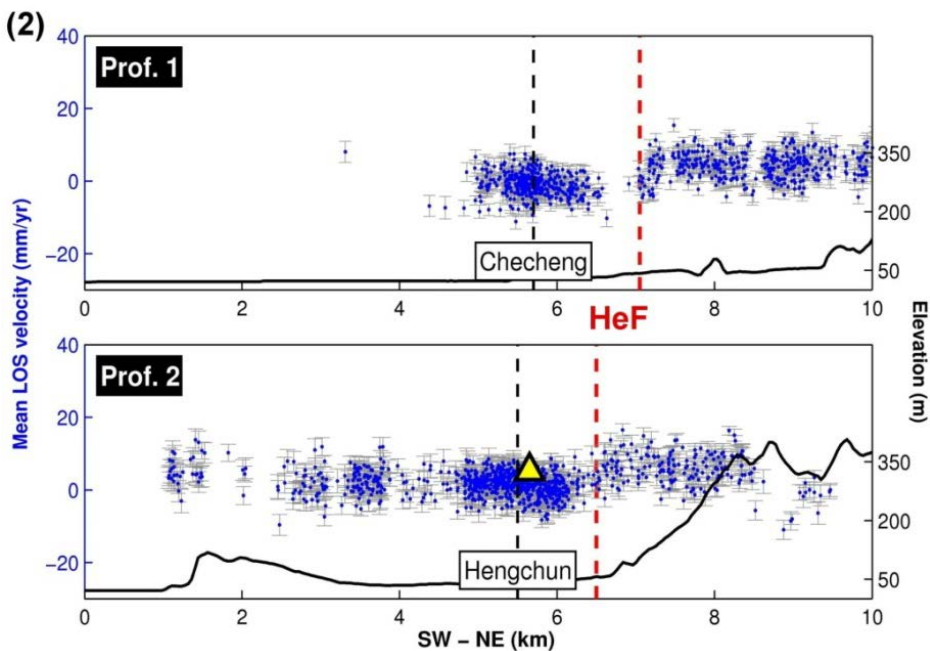
Figure 10: E-W projection of mean LOS velocity in mm/y (blue dots with error bars, E on the right) on profiles transverse to the Hengchun Valley, Black line: topography, Yellow triangle: GPS point, HeF: Hengchun Fault. Note on both profiles the LOS offsets close to 10 ± 2.5 mm y^{-1} associated with the Kenting Mélange uplift east of the Hengchun Fault which contrast with the
10 **relatively subsiding Hengchun valley.**
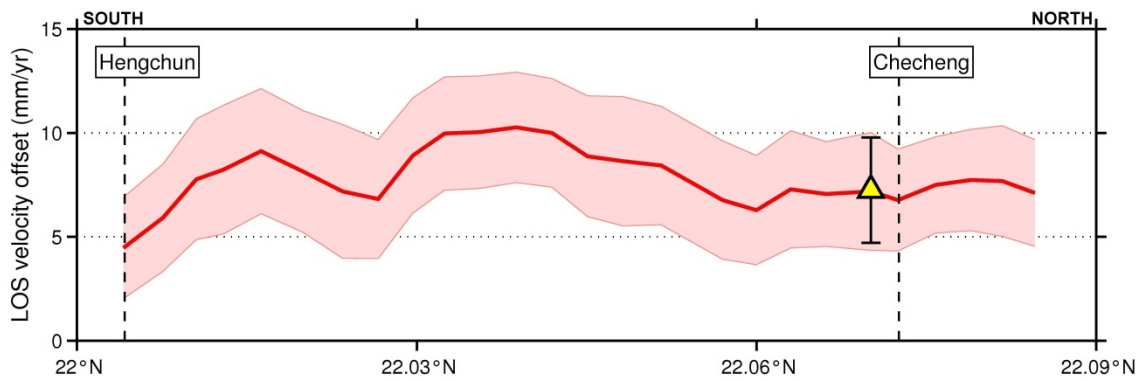
Figure 11: Hengchun Fault along strike variation of LOS velocity offset across Hengchun Fault (in mm y⁻¹) from Hengchun to Checheng cities. Note the active interseismic displacement and its northward variations which confirms that Hengchun fault is an active Fault of Taiwan.
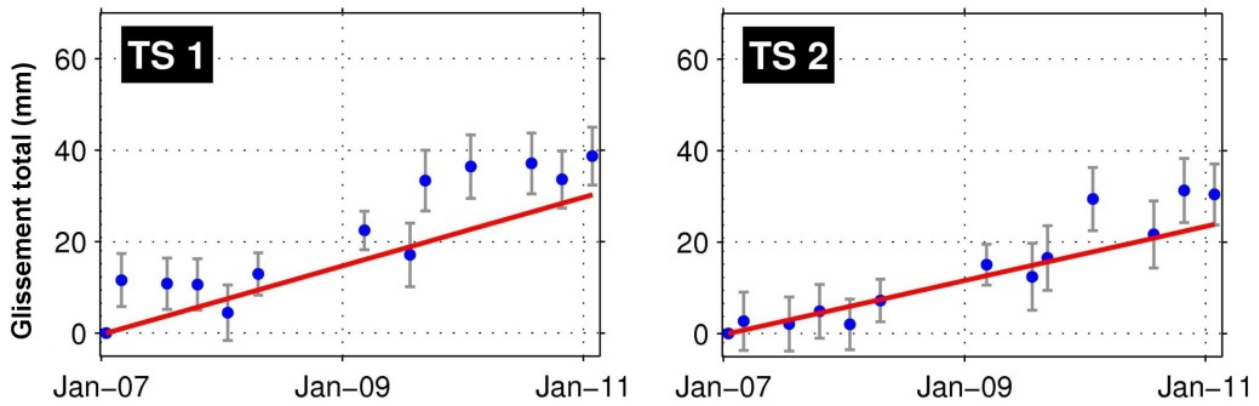
Figure 12: Time series of cumulated slip (on profiles 1 and 2) where no particular seasonal effects prevail. Further studies and PS monitoring ought to be developed in the near future to up-date and precise this aspect
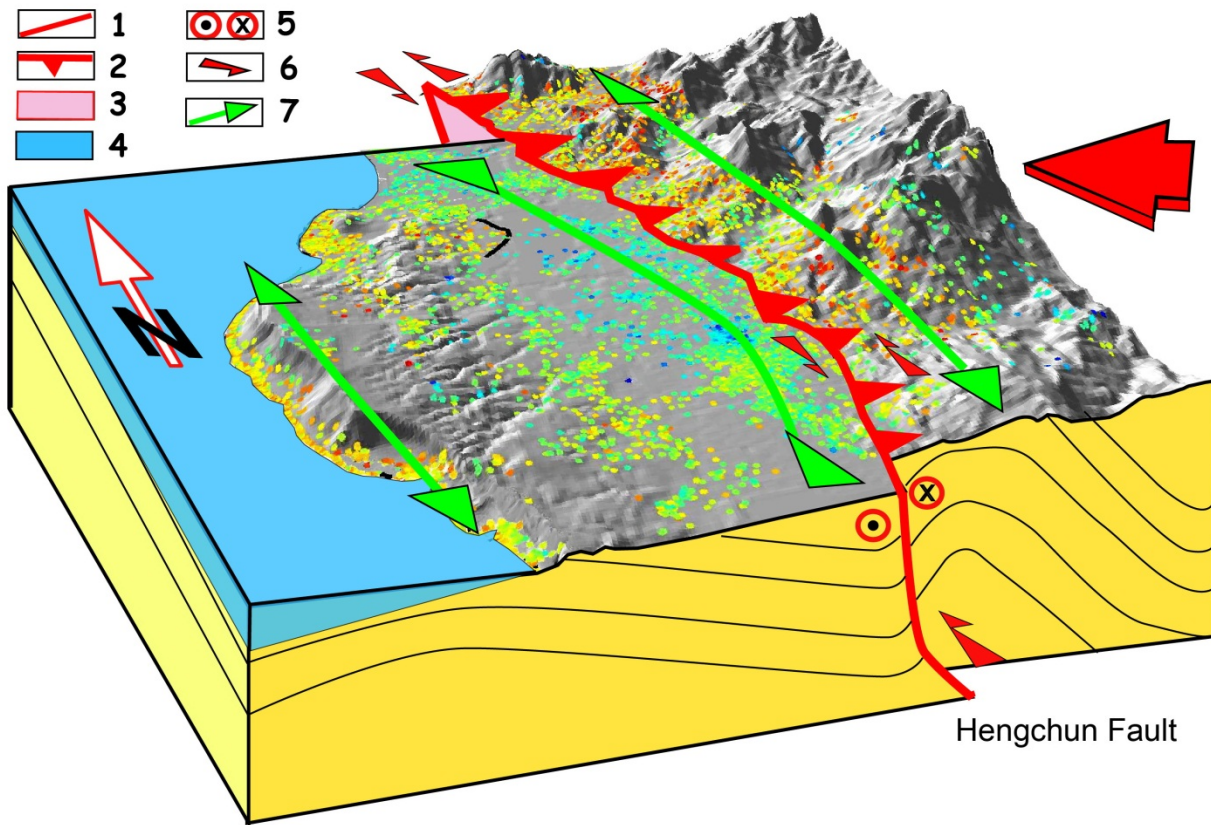
Figure 13: Simplest model of active inter-seismic tectonic deformation of the Hengchun Fault compatible with the oblique geodynamic convergence (large red arrow on the right), GPS and interferometric active displacements, and the detailed UAS DTM photo-interpretation. 1: Fault ; 2: Thrust ; 3: Fault plane ; 4: Taiwan Strait / South China Sea ; 5: Left lateral component ; 6: Transpressive left lateral component ; 7: Fold (anticline and syncline). The GPS data and PS mean LOS velocities implies that Hengchun Fault acts as a left-lateral transpressive strike-slip fault with an actively folding and uplifting anticline (hanging wall) contrasting with the aligned active subsidence of the syncline that trends parallel to the Hengchun Fault.